Heterogenization of Homogeneous Ruthenium(II) Catalysts for Carbon-Neutral Dehydrogenation of Polyalcohols

Ashley N. Hellman[a#], Nicole A. Torquato[a#], Michael E. Foster[a], Chaochao Dun[b], Joseph E. Reynolds III[a], Christine J. Yu[a], Andrew D. Tran[a], Mohana Shivanna[a], Gail Frances H. Garcia[a], Ji Yang[b], Yi Chen[b], Ji Su[b], Jeffrey J. Urban[b], Mark D. Allendorf[a]*, and Vitalie Stavila[a]*

[#] - *these authors contributed equally*

[a]Sandia National Laboratories, Livermore, California, 94551, United States

[b]Lawrence Berkeley National Laboratory, Berkeley, California, 94720, United States

*Email = mdallen@sandia.gov and vnstavi@sandia.gov

Abstract: Liquid organic hydrogen carrier (LOHC) systems are an excellent alternative to pressurized gas and liquid hydrogen storage technologies due to their high volumetric storage capacities and straightforward adaption to existing infrastructure. Homogeneous catalysts are promising for selective and reversible release of hydrogen from LOHC. However, separation from product mixtures and recycling inhibit their use, particularly when comprised of costly low-abundance elements, motivating the development of heterogeneous versions that are more easily recovered and reused. Here, we describe two methods for the heterogenization of molecular Ru catalysts that efficiently dehydrogenate the polyalcohol LOHCs ethylene glycol (EG) and 1,2-propanediol (1,2-PDO). The heterogeneous versions of these catalysts maintain catalytic activity for hydrogen production comparable to the homogeneous complexes, with up to 81% conversion and 99% selectivity. DFT modeling indicates mechanistic similarities for the dehydrogenations of EG and 1,2-PDO, with the rate-limiting steps associated with protonation of the Ru-H bond to form H_2 and the alkoxide-species coordinated to Ru(II),

followed by β-hydride elimination to regenerate the Ru-H bond. Overall, the data suggest these heterogenized molecular catalysts have potential for practical use in polyalcohol-based LOHC systems.

Keywords: *Liquid Organic Hydrogen Carriers, Heterogeneous catalysis, Reversible hydrogen storage, Ruthenium catalysts*

Introduction

Rapid population increases and the forecasted disastrous consequences of fossil fuel usage make the need for widespread clean energy sources paramount. The benefits of hydrogen as a carbon-neutral energy carrier are now widely recognized, with polymer electrolyte membrane fuel cells under serious consideration for transportation, stationary, and industrial uses.[1] In particular, liquid organic hydrogen carriers (LOHCs) are an emerging substitute for physical hydrogen storage (pressurized gas and liquid hydrogen) and transport due to the benefits of higher volumetric storage densities compared to compressed gas, lower costs, and reduced hazards compared to compressed or cryogenic hydrogen storage.[2, 3] Moreover, the facile integration of LOHCs with existing infrastructure is a major benefit that can reduce costs of storage and delivery from production to use.[1]

Various homogeneous hydrocarbon and nitrogen-containing aromatic systems have been considered as LOHCs, including methylcyclohexane-toluene and *N*-ethylcarbazole, among many others.[4, 5] However, many of these systems suffer from high cost and low gravimetric hydrogen storage capacity (HSCs) compared with other LOHCs such as alcohols.[6, 7] For example, methanol and ethanol are generally widely available, inexpensive, and are easily transported and stored. However, reversibility can be limited.[8] Molecules with an –OH functionality have the additional advantage of more highly activated bonds than hydrocarbons, allowing for hydrogen release

under milder conditions. Going a step further, polyalcohols display promising thermodynamics and undergo carbon neutral, non-volatile homocoupling reactions that form corresponding esters with high selectivity.

The literature contains extensive precedents for catalytic polyalcohol (or polyol) dehydrogenation, including ethylene glycol (EG),[9, 10] glycerol,[11-15] 1,4-butanediol,[16] 1,2-benzenedimethanol,[17, 18] and 1,2-propanediol (1,2 PDO),[19] which show activity for acceptorless dehydrogenation reactions using a variety of homogeneous Ir,[20] Fe,[17, 21] Ni,[22] Ru,[23, 24] and Mn[16, 25] pincer catalysts. Some of these were proposed as reversible LOHC systems.[8, 26, 27] Notably, EG, with a theoretical HSC of 6.5 wt%, is inexpensive due to its extensive use by the automotive industry as a refrigerant. EG reversibly releases hydrogen at up to 94% conversion when catalyzed by a variety of homogeneous Ru-pincer catalysts,[10, 28] making it an attractive option for reversible hydrogen storage.

Although there are benefits to using homogeneous catalysts, such as high diffusion and heat transfer rates, well-defined active sites, and directed tunability, they lack advantages of heterogeneous catalysts, including facile catalyst separation and recyclability. To combine the promising aspects of both classes of catalysts, homogeneous catalysts can be heterogenized onto a surface or within a defined structure; such catalysts have been employed for many chemical and electrochemical energy conversion reactions.[29-31] However, they have only recently been explored for acceptorless dehydrogenation reactions and LOHCs, selectively producing hydrogen but requiring high temperatures that limit practical applications.[32]

Herein we present two methods to heterogenize molecular ruthenium pincer catalysts, the Milstein Acridine Catalyst (Ru-9) and Ru-MACHO. Both are commercially available and are known to be efficient catalysts for reversible ethylene glycol[10] and ethanol dehydrogenation.[9, 33] Following characterization by porosimetry, X-ray photoelectron spectroscopy (XPS), and transmission electron microscopy-energy dispersive x-ray spectroscopy (TEM-EDS), the ability of these heterogeneous versions to catalyze EG

dehydrogenation (Scheme 1) was characterized. The results demonstrate catalytic activity analogous to the homogeneous complexes. Dehydrogenation activity toward several other polyalcohols is also shown, establishing that these heterogeneous platforms are applicable to a range of homogeneous complexes and polyalcohols. Catalytic activity was analyzed in depth, yielding kinetic and thermodynamic data supported by both experimental and theoretical studies. Overall, the data suggest that heterogenizing these molecular Ru catalysts creates versatile new nanoporous materials with comparable catalytic activity.

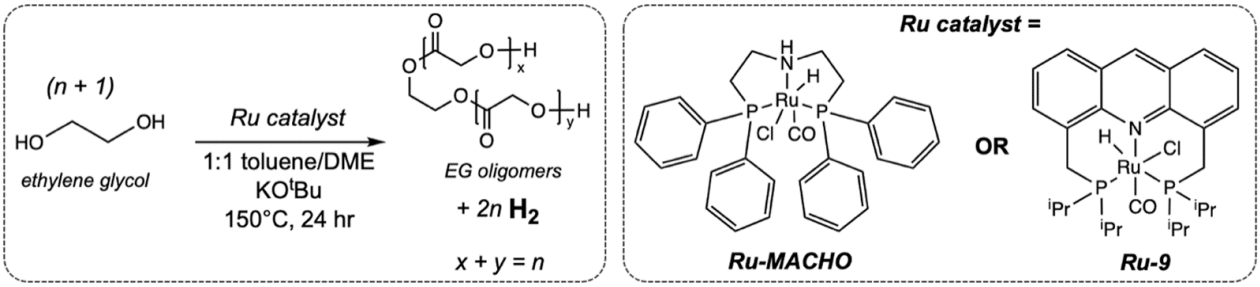

Scheme 1. Catalytic reaction scheme for the dehydrogenation of ethylene glycol to produce hydrogen using homogeneous catalysts Ru-MACHO and Ru-9.

Experimental and Computational Methods

The materials used, detailed characterization methods, and catalyst preparation methods are given in the Supporting Information.

General procedure for catalytic (de)hydrogenation of polyalcohols. Catalytic dehydrogenation reactions (Table 2) were assembled in an inert N_2 glove box. Catalyst loadings were 0.02 mmol of Ru-9 and Ru-MACHO catalysts for homogeneous reactions. The heterogeneous reactions were standardized relative to 0.02 mmol Ru (conjugated to support material) based on quantitative energy dispersive spectroscopy (EDS) measurements (Figures S1-S4). In addition to the catalyst, 0.04 mmol potassium tert-butoxide (KO^{t}Bu), 2.0 mmol of polyalcohol, 2 mL of 1:1 v/v toluene/2,2-

dimethyoxyethane (DME), and a stir bar were added to the reaction vessel. Catalytic solutions were sealed in a stainless steel 100 mL Parr autoclave with a magnetic stir bar and attached to a Parr reactor system, in which the reaction mixture was heated to 150 °C for 24-72 hours. Pressure and temperature were monitored throughout. After cooling to room temperature, the reactor was connected to rubber tubing and positioned in an inverted buret in a beaker of water; water displacement upon opening the reactor valve was used to measure gas production. The solution was then filtered and the precipate washed with acetone 4 x 0.5 mL. The precipate was dried and used for post-catalysis characterization by IR and quantitative EDS. The supernatant was also collected and the solvent removed under vacuum; mesitylene (140 µL, 1.0 mmol) was added as an internal standard. The residue was dissolved in acetone-d_6 and the resulting solution was passed through a 0.2 µm filter and then submitted for NMR analysis. Hydrogenation reactions used the same Parr autoclave containing the crude dehydrogenated reaction mixtures, including 0.02 mmol of the spent heterogenous Ru catalyst, toluene (1 ml), DME (1 ml), and a stir bar. The Parr autoclave was pressurized with 40 bar H_2 and heated to 150 °C for 48 hours. After cooling to room temperature, the autoclaves were transferred to a N_2 glovebox and opened. The reaction mixture was filtered and washed with THF. Workup was performed as described for dehydrogenation reactions.

General Procedures for Sieverts measurements. The dehydrogenation properties of neat ethylene glycol in the presence of Ru-MACHO-poly were measured using a pressure-composition-temperature (PCT, PCTPro-2000) volumetric apparatus. In this experiment, KO^{t}Bu (2.0 mg, 0.017 mmol), ethylene glycol (1.0000 g, 16.110 mmol), and Ru-Macho-poly (12.0 mg, 0.00843 mmol Ru) were added to a stainless-steel Sieverts reactor inside an argon glove-box. The reactor was sealed with a stainless-steel gasket, then connected to the PCTPro-2000 instrument. Helium gas (99.999% purity) was used for sample holder volume calibration. A thermocouple was placed in the center of the sample holder for accurate temperature measurements during

the experiments. Pressure changes during the dehydrogenation of the samples were quantified with calibrated pressure transducers and recorded by a LabView-based software program. The calculations of the wt% capacity assume hydrogen is the only gaseous product of the reaction.

Computational details. All calculations were performed using Gaussian 09.[34] Geometry optimization and frequency calculations involving Ru-9 and Ru-MACHO were performed at the DFT (ωB97XD/Def2-TZVP) level of theory.[35, 36] Note that the Cl atoms on Ru-9 and Ru-MACHO were removed; consequently, the systems were modeled in the cationic state. The frequency calculations were performed for a temperature of 150 °C (423.15 K) and all optimized geometries were confirmed to be either stationary points or transition states (one imaginary frequency). The modeled reaction pathways are based on the mechanism outlined for Ru-10.[10]

Results and Discussion

Reactions using homogeneous Ru catalysts

Prior to exploring methods for heterogenization, Ru-MACHO was investigated to establish its catalytic activity for polyol dehydrogenation and provide a baseline catalytic activity for the dehydrogenation of ethylene glycol (EG). These initial tests with the homogeneous catalysts were run at 150 °C with magnetic stirring and continuous pressure and temperature monitoring. Dehydrogenation of EG with Ru-MACHO resulted in a 59% NMR conversion of EG to higher molecular weight oligioesters, including hydroxyethyl glycolate, HEG, in 10% NMR yield, and the production of 26 mL of H_2 after 72 hours (Table 2, Figure S5). To determine the reversibility of the Ru-MACHO catalyst, the dehydrogenated reaction mixture was exposed to 40 bar H_2 at 150 °C. After 48 hours this led to the disappearance of oligomer

NMR peaks and conversion back to EG, indicating reversibility under these conditions (Figure S6).

In addition to EG, many other polyalcohols are inexpensive and have high theoretical hydrogen storage capacities.[8] As such, Ru-MACHO and Ru-9 were further investigated for the dehydrogenation of glycerol, 1,2-propanediol (1,2-PDO), and 1,3-propanediol (1,3-PDO). With both homogeneous catalysts, glycerol dehydrogenated to form moderate amounts of gas and conversion to a multitude of products as indicated by ^{1}H NMR, as reported previously.[37] Upon heating to 150 °C under 40 bar H_2, however, the dehydrogenated mixture underwent hydrogenolysis to produce a mixture of EG, 1,2-PDO, and water[38] (Figure S7). In contrast, 1,3-PDO produced low amounts of gas and generated clean products by NMR, but the dehydrogenation was not reversible, most likely due to decomposition (Figure S8). However, dehydrogenation of 1,2-PDO with Ru-MACHO was reversible, with gas production up to 20 mL (Table 2, Figure S9 and S10). Furthermore, Ru-9 dehydrogenation of 1,2 PDO resulted in 66% conversion to oligomers and 19 mL of H_2 (Table 2, Figure S11). Consequently, 1,2-PDO was selected with EG as substrates for experiments with heterogeneous Ru catalysts.

Heterogeneous Ru catalysts

Two different techniques for catalyst heterogenization were investigated for both Ru-9 and Ru-MACHO: 1) attachment to functionalized silica surfaces and 2) self-polymerization (Scheme 2). In the first approach, the aromatic backbones of the molecular complexes were immobilized on functionalized SBA-15 silica gel *via* a Mannich reaction, following literature precedent.[39] Infrared (IR) spectroscopy was initially employed to confirm attachment of each catalyst to the silica surface. However, due to the very small loadings of these silica-supported catalysts, the intensities of the carbonyl stretches are too low to determine successful attachment. A second reaction was performed using a higher concentration of Ru-MACHO (1:1 ratio of catalyst to

functionalized SBA-15); in this case, the IR spectrum does display a weak carbonyl stretch at 1911 cm^{-1}, similar to the peak at 1901 cm^{-1} in the spectrum of the molecular complex, demonstrating successful attachment of the catalyst to the functionalized surface (Figures S12 and S13).

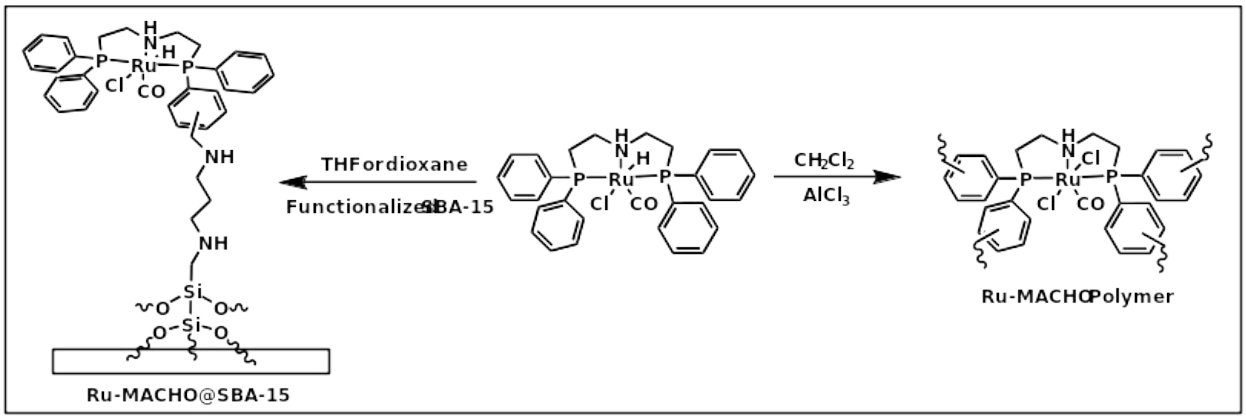

Scheme 2. Synthetic scheme for the two heterogenization methods, visualized using Ru-MACHO: functionalization on silica (left) and self-polymerization (right).

Molecular catalysts Ru-MACHO and Ru-9 were also self-polymerized via the phosphinophenyl ligands and acridine backbone, respectively, using a Lewis acid-catalyzed Friedel-Crafts reaction, with dichloromethane (DCM) acting as methylene donor and crosslinker (Scheme 2).[31] As the theoretical catalytic loadings of the Ru-9 and Ru-MACHO polymers are similar to those of the molecular catalysts due to the inclusion of a single additional methylene linker per catalyst unit, the IR spectra clearly display the carbonyl stretches indicating that the structural integrity of the molecular catalysts is preserved following polymerization. The CO stretch appears at 1944 cm^{-1} and 1941 cm^{-1} for Ru-MACHO-Poly and Ru-9-Poly, respectively (Figures S12 and S13). In comparison, the CO stretches of homogeneous Ru-MACHO and Ru-9 appear at 1911 cm^{-1} and 1887 cm^{-1}, respectively. Both molecules undergo a blue shift with self-polymerization, in agreement with the literature for Ru-MACHO-Poly.[31] This is due to the replacement of the hydride with an additional Cl atom, increasing the electronegativity on the Ru center. DFT calculations are consistent with this frequency shift in Ru-MACHO, predicting

that the CO stretch shifts from 1916 cm^{-1} to 1948 cm^{-1} upon replacement of H with Cl.

Additional characterization was performed to confirm successful heterogenization of each catalyst. Quantitative EDS measurements were obtained to determine the elemental composition of the heterogenized catalysts. These results demonstrate a higher Ru loading in Ru-MACHO-poly (7.1 wt% Ru) and Ru-9-poly (6.9 wt% Ru) than Ru-MACHO@SBA-15 (0.9 wt% Ru) and Ru-9@SBA-15 (0.6 wt% Ru) (Figures S1-S4). X-ray photoelectron spectroscopy (XPS) was performed to analyze the composition and surface structure. XPS spectra of both catalysts display all expected elements, including Ru, Si, P, Cl, N, P, and O (Figure 1 and S14-S21), indicating that the molecular structure of Ru-9 and Ru-MACHO within the heterogeneous frameworks is retained. Slight shifts in binding energies were observed (Figures S14-S21). These were relatively small and could not be unambiguously assigned to changes in chemical state or environment of the corresponding elements, as low catalyst loading or electrostatic effects may also contribute to the observed shifts. Both ruthenium and silicon were present in both SBA-supported catalysts, confirming successful attachment to the silica surfaces. Analysis of the deconvoluted Ru 3d spectra shows peaks corresponding to both Ru $3d_{3/2}$ and Ru $3d_{5/2}$, indicating that the Ru in each heterogeneous catalyst remains Ru(II), as in the molecular catalyst (Figure 1).

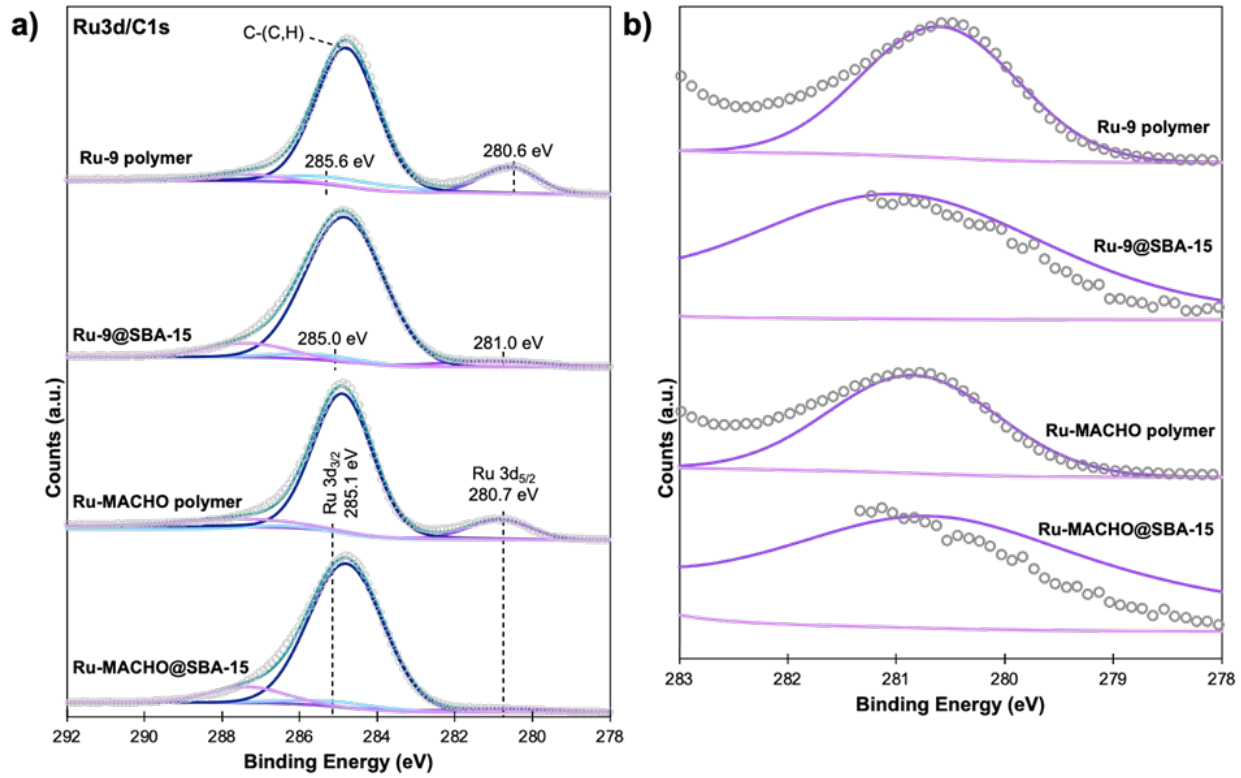

Figure 1. Deconvoluted Ru 3d and C 1s XPS data for Ru-based catalysts showing a) the full range of binding energy and b) the expanded range for Ru $3d_{5/2}$ peaks (relative scale increased for clarity).

The uniform distribution of the Ru-species throughout the catalyst particles was demonstrated by transmission electron microscopy (TEM) measurements using energy dispersive spectroscopy (EDS) (Figures 2 and S22-S25). The energy of the electrons used in TEM is high enough to probe the entire particle and not only its surface. High-angle annular dark-field (HAADF) TEM images are shown in the top row of Figure 2, with the EDS maps for Ru (yellow), P (purple), and Cl (blue) in the corresponding rows below. These elemental maps indicate that Ru, P, and Cl are dispersed throughout the catalyst particles. There is no evidence that Ru-species accumulate in a particular location or that catalyst decomposition occurs to form multiple species physically mixed with the catalyst particles. For the silica-supported catalysts, the silicon and oxygen peaks were also detected,

confirming the uniform distribution of the Ru-MACHO and Ru-9 species (Figures S22-S23).

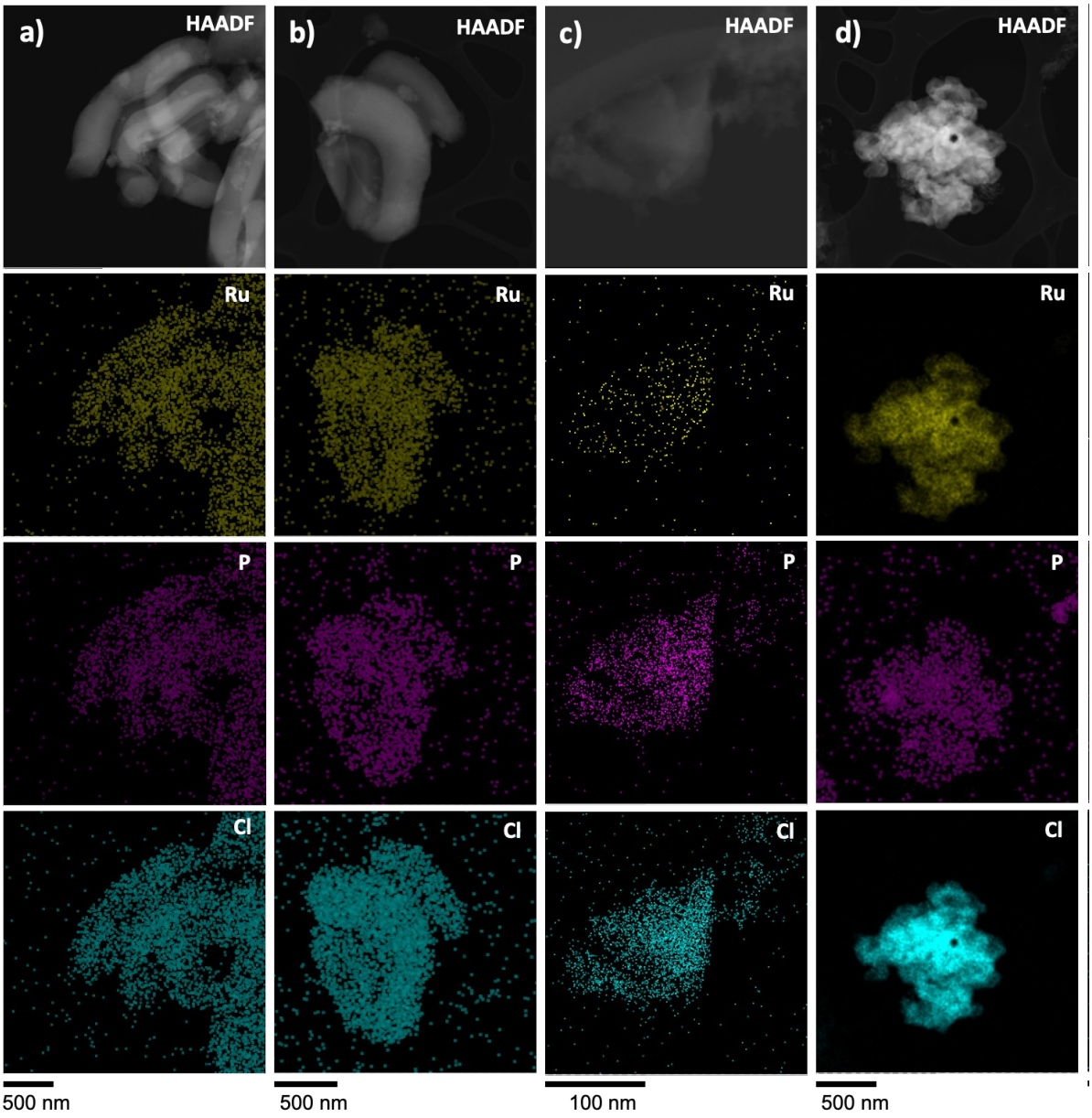

Figure 2. TEM/EDS data for Ru-based catalysts: a) Ru-MACHO@SBA-15, b) Ru-9@SBA-15, c) Ru-MACHO-Poly, and d) Ru-9-Poly. Scale bars are shown below each column.

Porosimetry was performed to determine the surface areas and pore sizes of the heterogenized catalysts (Figure S26). Brunauer–Emmett–Teller

(BET) surface areas, accessible pore volumes, and pore sizes (Table 1). Ru-MACHO@SBA-15 and Ru-9@SBA-15 were found to have similar surface areas (179 m^2/g and 161 m^2/g, respectively). Ru-MACHO-Poly has a surface area of 246 m^2/g and Ru-9-Poly has the highest surface area (366 m^2/g). Notably, all four catalysts have permanent porosity: their available pore volumes range from from 0.15 cm^3/g to 0.23 cm^3/g. The pore sizes of Ru-MACHO@SBA-15 and Ru-9@SBA-15 are the largest (48 Å and 50 Å, respectively). Those of Ru-MACHO-Poly and Ru-9-Poly are similar (24 and 25 Å, respectively) and are large enough for the polyalcohols and oligomers to diffuse through during catalysis, allowing for access to a greater number of active sites.

Table 1. Porosimetry data for the four heterogenized catalysts, showing BET surface area, pore volume, and pore size.

Catalyst	BET Surface Area (m^2/g)	Pore Volume (cm^3/g)	Pore Size (Å)
Ru-MACHO@SBA-15	179	0.214	47.8
Ru-9@SBA-15	161	0.203	50.3
Ru-MACHO-Poly	246	0.148	24.1
Ru-9-Poly	366	0.234	25.5

Following characterization, the activity of the heterogenized catalysts for dehydrogenation of EG to form H_2 was measured using the same conditions as the homogeneous catalysts. Previous reports of Ru-MACHO-Poly included an activation step (to remove Cl from the Ru complex) prior to dehydrogenation,[31] but our results indicate that the catalyst is active towards EG dehydrogenation even without the Cl removal step. The results of these experiments (Table 2) demonstrate that all four heterogeneous catalysts are active for EG dehydrogenation (Figures S27-S30). The resulting product mixtures exhibit similar NMR spectra and gas yields for EG dehydrogenation were comparable, with Ru-MACHO-poly and Ru-MACHO@SBA-15 having slightly better activity than the molecular Ru-MACHO catalyst (Table 2). The Ru-9 heterogenized catalysts (Ru-9@SBA-15 and Ru-9-poly) have slightly

lower activity than the homogeneous Ru-9 catalyst, with Ru-9@SBA-15 being the best heterogeneous EG dehydrogenation catalyst, with 81% conversion to oligioesters as shown by NMR and production of 34 mL of H_2. In the dehydrogenation of EG to oligioesters, the Ru-SBA-15 materials have low conversion to HEG (appx. 1%), whereas Ru-9-poly exhibits 12% HEG conversion and Ru-MACHO-poly 20% conversion to HEG (Figures S27-S30).

Table 2. Catalytic activity of 72-hour ethylene glycol and 1,2-propanediol dehydrogenation reactions using heterogenized molecular catalysts. Conversion values were calculated from quantitative NMR analysis utilizing mesitylene (1.0 mmol) as an internal standard. Conditions: 0.02 mmol Ru (conjugated to heterogeneous support material), 2 mmol EG, 1 mL toluene, 1 mL DME, 0.04 mmol KO^{t}Bu, 150 °C.
[a] Ref. 10

Catalyst	**Polyalcohol**	**Dehydrogenation**	
		NMR Conversion (%)	Gas volume (mL)
Ru-9	EG	94[a]	54[a]
	1,2-PDO	66	19
Ru-MACHO	EG	59	26
	1,2-PDO	65	20
Ru-9@SBA-15	EG	81	34
	1,2-PDO	68	21
Ru-MACHO@SBA-15	EG	66	30
	1,2-PDO	67	24
Ru-9-Poly	EG	56	25
	1,2-PDO	65	23
Ru-MACHO-Poly	EG	63	31
	1,2-PDO	70	25

NMR conversion and gas volumes for 1,2 PDO dehydrogenation are comparable among the heterogeneous catalysts and show slightly higher activity than the homogeneous analogs (Table 2, Figures S31-S34). Among the catalysts for 1,2 PDO dehydrogenation, Ru-MACHO-poly has the best performance, with 70% conversion to olioesters and the production of 25 mL H_2.

Following the dehydrogenation reactions, IR and quantitative EDS analysis of the heterogenous catalysts demonstrate retention of Ru in the

catalyst manifold (Figures S35-S42). In addition, post-reaction inductively coupled plasma (ICP) measurements of the catalytic solutions yielded no evidence of Ru, indicating there is no Ru leaching during the catalytic processes using these heterogenized catalysts.

We determined the reaction thermodynamics from a Van't Hoff plot (Figures 3 and S43-S44), using the reactor pressure measured once the temperature stabilized in the presence of excess amounts of polyalcohols. The ΔH and ΔS values obtained for EG and 1,2-PDO (using Ru-MACHO-Poly) are given in Table 3. The enthalpy values are consistent with ΔH for the dehydrogenation of ethanol (36 kJ/mol).[40] The enthalpy and entropy values for EG and 1,2-PDO are nearly the same.

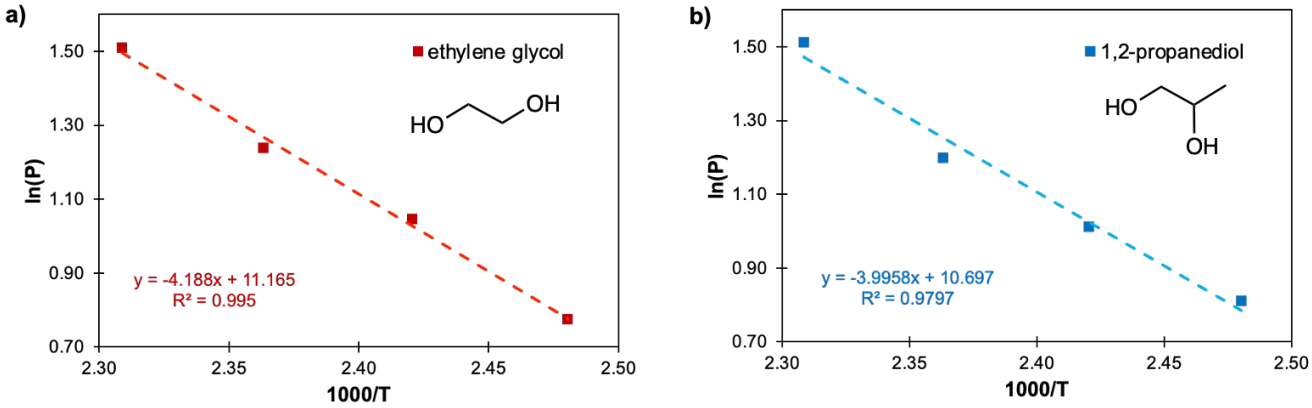

Figure 3. Van't Hoff plot showing ln(P) vs. 1000/T using Parr reactor data from catalytic dehydrogenations of a) EG and b) 1,2-PDO with Ru-MACHO-Poly.

Table 3. Experimental thermodynamic data for the dehydrogenation of EG and 1,2-PDO, collected using Ru-MACHO-Poly as catalyst.

Polyalcohol	**ΔH (kJ/mol)**	**ΔS (J/mol•K)**	**ΔG (kJ/mol)**
Ethylene Glycol	34.8	92.8	-4.5
1,2-Propanediol	33.2	88.9	-4.4

Ru-MACHO-Poly was selected for more detailed catalytic studies as it uses the cheaper Ru-MACHO precursor and the synthesis is easily scaled up. Gas chromatography (GC) studies were performed following catalytic reactions with Ru-MACHO-Poly to determine the purity of the gas produced from each polyalcohol. These studies demonstrated that dehydrogenation of EG and 1,2-PDO produced only H_2.

Additional GC studies were performed for both EG and 1,2-PDO at several temperatures (130 °C, 150 °C, and 170 °C), during which the Parr vessel was opened for GC analysis at several time points and closed upon gas release. These experiments again indicated that only H_2 was produced, even when changing from a closed to a partially open system. As expected, both diols produced greater amounts of gas at higher temperatures, with the rates of gas production increasing as well. Dehydrogenation of 1,2-PDO produced more gas with faster rates at all temperatures (Figures 4 and S45. Activation energies (E_a) calculated using the Arrhenius equation were determined to be 124 kJ/mol and 61 kJ/mol for EG and 1,2-PDO, respectively (Figure S46).

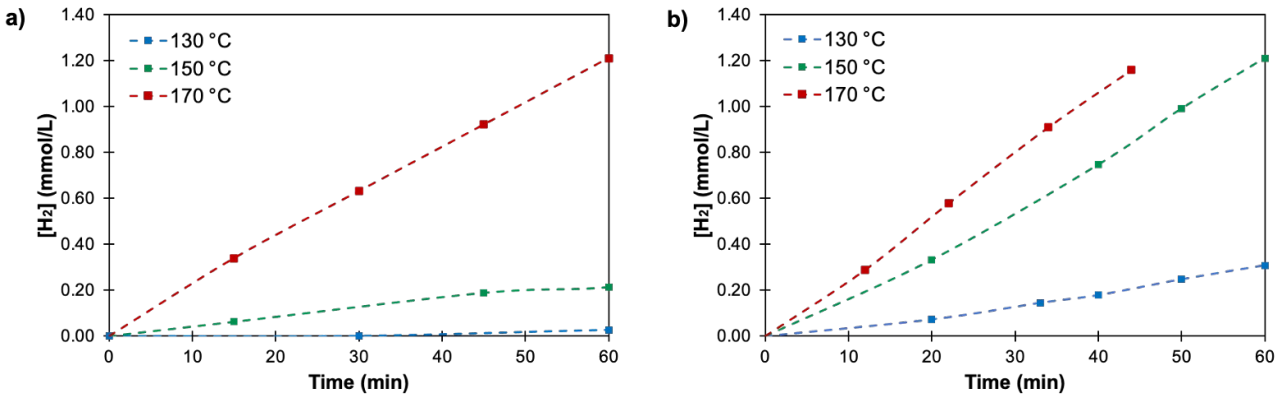

Figure 4. Kinetic studies of the dehydrogenation of (a) ethylene glycol and (b) 1,2-propanediol with Ru-MACHO-Poly showing hydrogen production over time at 130 °C (grey), 150 °C (red), and 170 °C (blue), as determined by gas chromatography. Plots are normalized to show hydrogen production under isothermal conditions.

Although the measured activation energies for EG and 1,2-PDO are two to three times greater than those of some alcohol dehydrogenations (e.g. benzyl alcohol) using heterogeneous catalysts, they are closer to other reported E_a values, such as for the dehydrogenation of methanol to methyl formate and the dehydrogenation of cyclohexanol using heterogeneous catalysts (Table S1).[41-47] In general, the O-H bonds of polyols are more stable and difficult to activate, making the successful dehydrogenation of EG and 1,2-PDO using our heterogenized molecular catalysts noteworthy.

From an industrial standpoint, solvent-free reaction conditions are advantageous due to decreased reaction time, lower energy consumption, and an increased hydrogen capacity of the system. Consequently, we investigated the long-term catalyst stability, reversibility, and recyclability of Ru-MACHO-poly under neat conditions. The cycle-life catalytic measurements were performed using the Sieverts technique with Ru-MACHO-Poly. Catalytic solutions of neat EG (1.000 g, 16.11 mmol), KO^{t}Bu (2.0 mg, 0.018 mmol), and Ru-MACHO-Poly (12.0 mg, 0.00843 mmol) were loaded into a stainless steel reactor and heated from RT to temperatures within the range of 144 to 155 °C for five consecutive dehydrogenations. After the reaction was cooled down to RT, the catalyst was recovered and washed with DME/toluene after each cycle and fresh EG and KO^{t}Bu were added for each subsequent cycle. The reaction mixture was then reheated for the next dehydrogenation reaction. Again unsurprisingly, higher reaction temperatures led to greater hydrogen production (Figure 5a). Ru-MACHO-Poly is fully recoverable and reversible in the reaction, with no apparent loss of catalytic dehydrogenation efficiency. Post-catalytic residual gas analysis shows production of only gaseous hydrogen (m/z = 2) with trace water (m/z = 18), confirming the GC results that this reaction is selective for the formation of H_2 (Figure 5b).

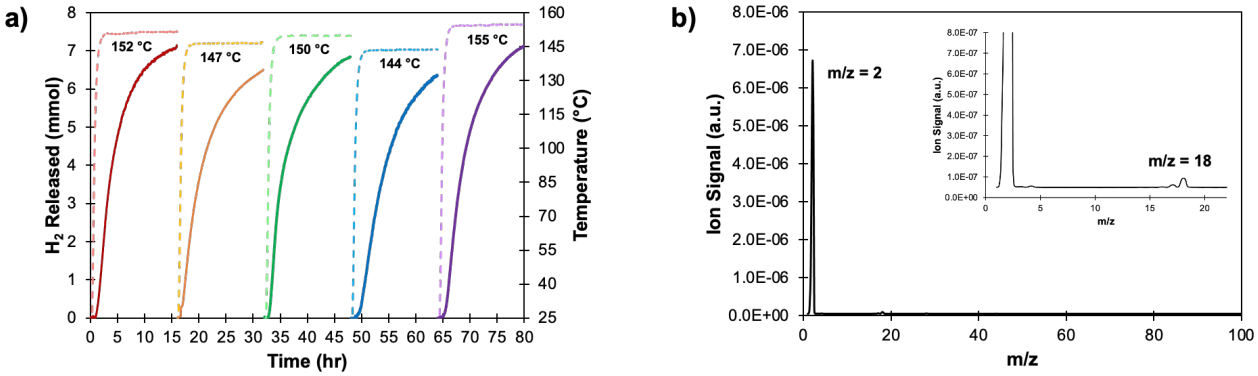

Figure 5. a) Sieverts plots displaying H_2 released and temperature (dashed line) as a function of time across five consecutive catalytic EG dehydrogenation cycles and b) RGA plot for product analysis after EG dehydrogenation, both using Ru-MACHO-Poly.

Computational Results

Density functional theory (DFT) was used to gain insight into the mechanism of the dehydrogenation of EG catalyzed by Ru-MACHO and Ru-9. The results are summarized in Figures 6 and S47 and illustrate the proposed mechanism to produce H_2 and 2-hydroxyethyl glycolate (HEG; EG dimer) using Ru-MACHO and Ru-9, respectively. The first step involves the removal of the Cl atom from the catalysts, producing a five-coordinate complex; this step is not modeled but occurs because of the presence of KO^{t}Bu in the reaction. Moreover, the removal of Cl is required for EG to interact with the Ru atom of the catalyst. The next step (first step modeled), is the binding of EG to the catalyst (intermediate A), followed by protonation of the Ru-H bond (transition state AB (TS_{AB})), yielding H_2 and a κ^2-alkoxidecoordinated complex, B. Next, the hydroxo bond is broken, followed by β-hydride elimination (TS_{BC}), regenerating the Ru-H bond (complex C). Upon addition of another EG, dehydrogenation proceeds (via TS_{CD}), yielding complex D. A subsequent β-hydride elimination (TS_{DE}) results in a metal-bound ester (complex E); finally, HEG is released, and the catalyst is restored to its active

form. These steps are based on the mechanism previously reported/proposed for Ru-10.[10]

The most important steps in the dehydrogenation process are the highest-energy TS and the lowest-energy intermediate. The former is the largest energy barrier that must be surmounted for the reaction to proceed and the latter is relevant because if an intermediate is too strongly bound, the reaction rate will decrease. Our modeling indicates that the largest reaction barrier is TS_{AB} (the first protonation of the Ru—H bond). For EG dehydrogenation catalyzed by Ru-MACHO and Ru-9, the barriers are predicted to be 111 and 73.3 kJ/mol, respectively. In addition to the larger energy barrier associated with EG@Ru-MACHO, the intermediates are more strongly bound (see Figures 6 & S47 and Table 4). Based on these results, Ru-9 is predicted to be a more active catalyst for the dehydrogenation of EG; this conclusion is consistent with our experimental findings.

Table 4. Ethylene glycol (EG) and 1,2-propanediol (1,2-PDO) binding energies (BE) to Ru-MACHO and Ru-9 and the first transition state (TS) energies involved in the dehydrogenation processes (see Figures 6 and S47). Gibbs free energies at 423.15 K were used in all cases. All values are in kJ/mol.

		wB97X-D/def2TZV		
		Intermediate A	TS_{AB}	Intermediate B
Ru-MACHO	EG	-57.5	111	-86.7
	1,2-PDO	-48.7	114	-82.0
Ru-9	EG	-19.5	73.3	-64.4
	1,2-PDO	-17.7	98.7	-60.7

Given that the first three steps appear to be rate-determining (largest TS; most strongly bound intermediates) in the dehydrogenation process, these steps were also modeled for 1,2-PDO interacting with Ru-MACHO and Ru-9. The binding energies (intermediates A and B) and the first transition state (TS_{AB}) are tabulated in Table 4. The TS and binding energies are similar for 1,2-PDO and EG; this is not surprising given the structural similarities. The

only difference between 1,2-PDO and EG lies in energy of the transition state TS_{AB} with Ru-9, which is predicted to be ~20 kJ/mol higher in energy for 1,2-PDO then for EG. Although we cannot rule out the possibility that a lower-energy transition state exists, this difference in activation barriers is consistent with the greater steric hindrance around the Ru atom in Ru-9 than in Ru-MACHO. This could impede access of 1,2-PDO, which is a slightly larger molecule than EG. Based on these results, we do not expect gas production from EG to be significantly different from 1,2-PDO, which again is consistent with our experimental results.

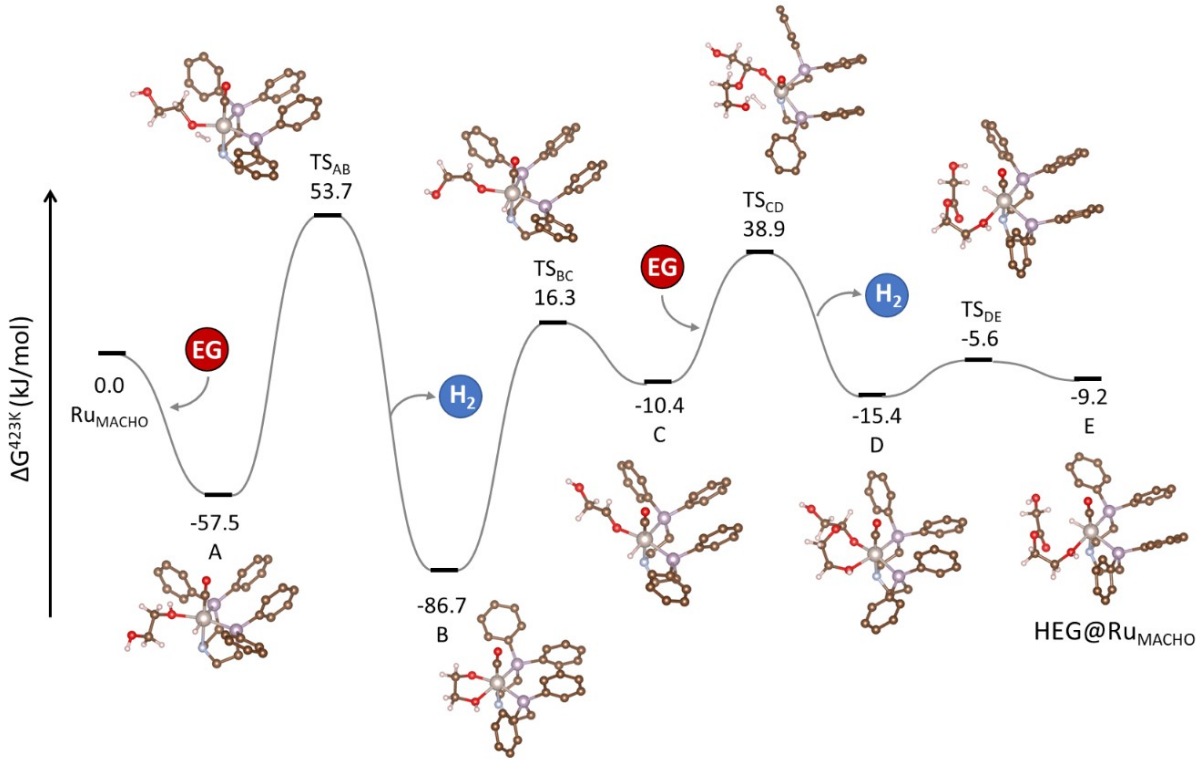

Figure 6. A schematic of the proposed catalytic cycle for the formation of a HEG with Ru-MACHO. Values correspond to Gibbs free energies (kJ/mol; wrt Ru-MACHO w/o Cl) at 423.15 K. H atoms on Ru-MACHO, except Ru-H, are omitted for clarity. Brown, carbon; purple, phosphorous; red, oxygen; sliver, ruthenium; blue, nitrogen; white, hydrogen.

Conclusions

The results just described demonstrate the successful heterogenization of two commercially available organometallic Ru(II) catalysts, Ru-9 and Ru-

MACHO, by two different methods: silica mounting and self-polymerization. FT-IR, XPS, and quantitative EDS measurements confirm catalyst incorporation and TEM/EDS illustrates uniform catalyst dispersion within the various platforms. We anticipate that these platforms are sufficiently general that they can be applied to a range of metal pincer catalysts to improve their performance and reduce the cost of polyols as LOHCs.

The four heterogeneous molecular catalysts were employed for the dehydrogenation of polyalcohols. EG and 1,2 PDO exhibit selective hydrogen production and catalytic activity (up to 81% conversion and 99% selectivity) analogous to that of the homogeneous versions. Moreover, post-dehydrogenation washing and replenishing of the reaction solution resulting from Ru-MACHO-poly catalysis yielded stable activity for at least five consecutive dehydrogenation reactions, highlighting the durability and recyclability of this catalyst.

Our DFT calculations are consistent with the experimental results, indicating that the catalysts have high affinity towards both EG and 1,2-PDO. Combining this result with the high porosity of these solid-supported catalysts suggests that the heterogeneous catalysts can preconcentrate the reagents within the pores. The calculations also indicate that the first transition state (initial formation of H_2) has the highest energy barrier and that the overall activation energy is larger for Ru-MACHO than for Ru-9, whereas EG has a lower energy barrier for dehydrogenation than 1,2-PDO. These trends are in general agreement with the experimental findings.

To date, the reversible catalytic dehydrogenation of polyols has only been demonstrated using homogeneous catalysts.[10] Our studies show that the heterogeneous versions of Ru pincer catalysts maintain analogous catalytic activity for H_2 generation and can thus be an alternative to the molecular versions. The two heterogenization techniques preserve the molecular catalytic structures and should thus be applicable to a diverse array of homogeneous catalysts containing phenyl or other aromatic groups. Many commercial and facilely synthesizable organometallic complexes exist

that could be readily heterogenized by these methods, in particular the self-polymerization approach. The two heterogenization strategies should also be applicable to other energy storage and sustainable catalytic processes, such as heterocoupling dehydrogenations,[9, 16, 24, 48] CO_2 capture and conversion,[49-51] and biomass valorization.[7, 52, 53] This motivates follow-on investigations in which the homogeneous catalysts is modified by changing the metal center, ligands, functional groups, and catalyst loadings. Modifications to the silica supports to tailor pore size and surface area should also be considered. Finally, by targeting the energy barrier for the first transition state these alterations can improve the reaction kinetics, allowing for higher gas production and further increasing long-term stability. Such advances are necessary so that polyol-based LOHCs can be a component of strategies under development to effectively address the demand for renewable hydrogen.

Supporting Information

Detailed experimental methods; characterization methods; quantitative EDS; ^{1}H NMR spectroscopy; FT-IR; XPS; HAADF-EDS; BET porosity measurements; kinetic studies; and the proposed catalytic cycle for the formation of HEG with Ru-9.

Author Information

Corresponding Authors:

Mark D. Allendorf – *Sandia National Laboratories, Livermore, CA, 94551, United States*; Email: mdallen@sandia.gov

Vitalie Stavila – *Sandia National Laboratories, Livermore, CA, 94551, United States*; Email: vnstavi@sandia.gov

Authors:

Ashley N. Hellman – *Sandia National Laboratories, Livermore, CA, 94551, United States*

Nicole A. Torquato – *Sandia National Laboratories, Livermore, CA, 94551, United States*
Michael E. Foster – *Sandia National Laboratories, Livermore, CA, 94551, United States*
Chaochao Dun – *Lawrence Berkeley National Laboratory, Berkeley, CA, 94720, United States*
Joseph E. Reynolds III – *Sandia National Laboratories, Livermore, CA, 94551, United States*
Christine J. Yu – *Sandia National Laboratories, Livermore, CA, 94551, United States*
Andrew D. Tran – *Sandia National Laboratories, Livermore, CA, 94551, United States*
Mohana Shivanna – *Sandia National Laboratories, Livermore, CA, 94551, United States*
Gail Frances H. Garcia – *Sandia National Laboratories, Livermore, CA, 94551, United States*
Ji Yang – *Lawrence Berkeley National Laboratory, Berkeley, CA, 94720, United States*
Yi Chen – *Lawrence Berkeley National Laboratory, Berkeley, CA, 94720, United States*
Ji Su – *Lawrence Berkeley National Laboratory, Berkeley, CA, 94720, United States*
Jeffrey J. Urban – *Lawrence Berkeley National Laboratory, Berkeley, CA, 94720, United States*

Notes. The authors declare no competing financial interest.

Acknowledgments

The authors acknowledge financial support through the Hydrogen Storage Materials Advanced Research Consortium (HyMARC) of the U.S. Department of Energy (DOE), Office of Energy Efficiency and Renewable

Energy, Fuel Cell Technologies Office under Contracts DE-AC52-07NA27344 and DE-AC04-94AL85000. Sandia National Laboratories is a multi-mission laboratory managed by National Technology and Engineering Solutions of Sandia, LLC, a wholly owned subsidiary of Honeywell International Inc., for the DOE's National Nuclear Security Administration under contract DE-NA0003525. Studies at the Molecular Foundry of the Lawrence Berkeley National Laboratory were supported by the Office of Science, Office of Basic Energy Sciences, of the U.S. Department of Energy under Contract No. DE-AC02-05CH11231. The authors would also like to acknowledge Robert Horton, Austin Acosta, and Walter Ramirez for their assistance and useful discussions.

References:

(1) Allendorf, M. D.; Stavila, V.; Snider, J. L.; Witman, M.; Bowden, M. E.; Brooks, K.; Tran, B. L.; Autrey, T. Challenges to developing materials for the transport and storage of hydrogen. *Nat. Chem.* **2022**, *14*, 1214-1223.

(2) Preuster, P. A., A.; Wasserscheid, P. Hydrogen Storage Technologies for Future Energy Systems. *Annu. Rev. Chem. Biomol. Eng.* **2017**, *8*, 445-471.

(3) Rao, P.; Yoon, M. Potential Liquid-Organic Hydrogen Carrier (LOHC) Systems: A Review on Recent Progress. *Energies* **2020**, *13*, 1-23.

(4) Teichmann, D.; Arlt, W.; Wasserscheid, P.; Freymann, R. A future energy supply based on Liquid Organic Hydrogen Carriers (LOHC). *Energy Env. Sci.* **2011**, *4*, 2767-2773.

(5) Modisha, P. M.; Ouma, C. N. M.; Garidzirai, R.; Wasserscheid, P.; Bessarabov, D. The Prospect of Hydrogen Storage Using Liquid Organic Hydrogen Carriers. *Energy & Fuels* **2019**, *33*, 2778-2796.

(6) Sekine, Y.; Higo, T. Recent Trends on the Dehydrogenation Catalysis of Liquid Organic Hydrogen Carrier (LOHC): A Review. *Top. Catal.* **2021**, *64*, 470-480.

(7) Ferlin, F.; Valentini, F.; Marrocchi, A.; Vaccaro, L. Catalytic Biomass Upgrading Exploiting Liquid Organic Hydrogen Carriers (LOHCs). *ACS Sustain. Chem. Eng.* **2021**, *9*, 9604-9624.

(8) Trincado, M.; Bösken, J.; Grützmacher, H. Homogeneously catalyzed acceptorless dehydrogenation of alcohols: A progress report. *Coord. Chem. Rev.* **2021**, *443*, 213967.

(9) Zhou, Q. Q.; Zou, Y. Q.; Ben-David, Y.; Milstein, D. A Reversible Liquid-to-Liquid Organic Hydrogen Carrier System Based on Ethylene Glycol and Ethanol. *Chemistry* **2020**, *26*, 15487-15490.

(10) Zou, Y. Q.; von Wolff, N.; Anaby, A.; Xie, Y.; Milstein, D. Ethylene Glycol as an Efficient and Reversible Liquid Organic Hydrogen Carrier. *Nat. Catal.* **2019**, *2*, 415-422.

(11) Lu, Z.; Demianets, I.; Hamze, R.; Terrile, N. J.; Williams, T. J. A Prolific Catalyst for Selective Conversion of Neat Glycerol to Lactic Acid. *ACS Catal.* **2016**, *6*, 2014-2017.

(12) Sharninghausen, L. S.; Mercado, B. Q.; Crabtree, R. H.; Hazari, N. Selective conversion of glycerol to lactic acid with iron pincer precatalysts. *Chem. Commun.* **2015**, *51*, 16201-16204.

(13) Li, Y.; Nielsen, M.; Li, B.; Dixneuf, P. H.; Junge, H.; Beller, M. Ruthenium-catalyzed hydrogen generation from glycerol and selective synthesis of lactic acid. *Green Chem.* **2015**, *17*, 193-198.

(14) Bottari, G.; Barta, K. Lactic acid and hydrogen from glycerol via acceptorless dehydrogenation using homogeneous catalysts. *Recyclable Catal.* **2015**, *2*, 70-77.

(15) Sharninghausen, L. S.; Campos, J.; Manas, M. G.; Crabtree, R. H. Efficient selective and atom economic catalytic conversion of glycerol to lactic acid. *Nat. Commun.* **2014**, *5*, 5084-5092.

(16) Nguyen, D. H.; Trivelli, X.; Capet, F.; Paul, J.-F.; Dumeignil, F.; Gauvin, R. M. Manganese Pincer Complexes for the Base-Free, Acceptorless Dehydrogenative Coupling of Alcohols to Esters: Development, Scope, and Understanding. *ACS Catal.* **2017**, *7*, 2022-2032.

(17) Bonitatibus, P. J., Jr.; Chakraborty, S.; Doherty, M. D.; Siclovan, O.; Jones, W. D.; Soloveichik, G. L. Reversible catalytic dehydrogenation of alcohols for energy storage. *Proc. Natl. Acad. Sci.* **2015**, *112*, 1687-1692.

(18) Musa, S.; Shaposhnikov, I.; Cohen, S.; Gelman, D. Ligand-metal cooperation in PCP pincer complexes: rational design and catalytic activity in acceptorless dehydrogenation of alcohols. *Angew. Chem. Int. Ed.* **2011**, *50*, 3533-3537.

(19) Weber, M. A.; Ford, P. C. Catalytic dehydrogenation of 1,2- and 1,3-diols. *J. Mol. Catal. A. Chem.* **2016**, *416*, 81-87.

(20) Ngo, A. H.; Adams, M. J.; Do, L. H. Selective Acceptorless Dehydrogenation and Hydrogenation by Iridium Catalysts Enabling Facile Interconversion of Glucocorticoids. *Organometallics* **2014**, *33*, 6742-6745.

(21) Chakraborty, S.; Lagaditis, P. O.; Förster, M.; Bielinski, E. A.; Hazari, N.; Holthausen, M. C.; Jones, W. D.; Schneider, S. Well-Defined Iron Catalysts for the Acceptorless Reversible Dehydrogenation-Hydrogenation of Alcohols and Ketones. *ACS Catal.* **2014**, *4*, 3994-4003.

(22) Chakraborty, S.; Piszel, P. E.; Brennessel, W. W.; Jones, W. D. A Single Nickel Catalyst for the Acceptorless Dehydrogenation of Alcohols and Hydrogenation of Carbonyl Compounds. *Organometallics* **2015**, *34*, 5203-5206.

(23) Tseng, K.-N. T.; Kampf, J. W.; Szymczak, N. K. Base-Free, Acceptorless, and Chemoselective Alcohol Dehydrogenation Catalyzed by an Amide-Derived NNN-Ruthenium(II) Hydride Complex. *Organometallics* **2013**, *32*, 2046-2049.

(24) Chang, W.; Gong, X.; Wang, S.; Xiao, L. P.; Song, G. Acceptorless dehydrogenation and dehydrogenative coupling of alcohols catalysed by protic NHC ruthenium complexes. *Org. Biomol. Chem.* **2017**, *15*, 3466-3471.

(25) Shao, Z.; Wang, Y.; Liu, Y.; Wang, Q.; Fu, X.; Liu, Q. A general and efficient Mn-catalyzed acceptorless dehydrogenative coupling of alcohols with hydroxides into carboxylates. *Org. Chem. Front.* **2018**, *5*, 1248-1256.

(26) Chandra, P.; Ghosh, T.; Choudhary, N.; Mohammad, A.; Mobin, S. M. Recent advancement in oxidation or acceptorless dehydrogenation of alcohols to valorised products using manganese based catalysts. *Coord. Chem. Rev.* **2020**, *411*, 213241-213299.

(27) Crabtree, R. H. Homogeneous Transition Metal Catalysis of Acceptorless Dehydrogenative Alcohol Oxidation: Applications in Hydrogen Storage and to Heterocycle Synthesis. .*Chem. Rev.* **2017**, *117*, 9228-9246.

(28) Yue, H.; Zhao, Y.; Ma, X.; Gong, J. Ethylene glycol: properties, synthesis, and applications. *Chem. Soc. Rev.* **2012**, *41*, 4218-4244.

(29) Corbin, N.; Zeng, J.; Williams, K.; Manthiram, K. Heterogeneous molecular catalysts for electrocatalytic CO2 reduction. *Nano Res.* **2019**, *12*, 2093-2125..

(30) Wang, J.; Dou, S.; Wang, X. Structural tuning of heterogeneous molecular catalysts for electrochemical energy conversion. *Sci. Adv.* **2021**, *7*, 1-13.

(31) Padmanaban, S.; Gunasekar, G. H.; Yoon, S. Direct Heterogenization of the Ru-Macho Catalyst for the Chemoselective Hydrogenation of alpha,beta-Unsaturated Carbonyl Compounds. *Inorg. Chem.* **2021**, *60*, 6881-6888.

(32) Polukeev, A. V.; Wallenberg, R.; Uhlig, J.; Hulteberg, C. P.; Wendt, O. F. Iridium-Catalyzed Dehydrogenation in a Continuous Flow Reactor for Practical On-Board Hydrogen Generation From Liquid Organic Hydrogen Carriers. *ChemSusChem* **2022**, *15*, 1-10.

(33) Nielsen, M.; Junge, H.; Kammer, A.; Beller, M. Towards a Green Process for Bulk-Scale Synthesis of Ethyl Acetate: Efficient Acceptorless Dehydrogenation of Ethanol. *Angew. Chem. Int. Ed.* **2012**, *51*, 5711-5713.

(34) *Gaussian 09*; Gaussian, Inc.: Wallingford CT, 2009. (accessed on 05/05/2023).

(35) Chai, J. D.; Head-Gordon, M. Long-range corrected hybrid density functionals with damped atom-atom dispersion corrections. *Phys. Chem. Chem. Phys.* **2008**, *10*, 6615-6620.

(36) Weigend, F.; Ahlrichs, R. Balanced basis sets of split valence, triple zeta valence and quadruple zeta valence quality for H to Rn: Design and assessment of accuracy. *Phys. Chem. Chem. Phys.* **2005**, *7*, 3297-3305.

(37) Valter, M.; Santos, E. C. d.; Pettersson, L. G. M.; Hellman, A. Selectivity of the First Two Glycerol Dehydrogenation Steps Determined Using Scaling Relationships. *ACS Catal.* **2021**, *11*, 3487-3497.

(38) Dasari, M. A.; Kiatsimkul, P.-P.; Sutterlin, W. R.; Suppes, G. J. Low-pressure hydrogenolysis of glycerol to propylene glycol. *Appl. Catal. A: Gen.* **2005**, *281*, 225-231.

(39) Goni, M. A.; Rosenberg, E.; Gobetto, R.; Chierotti, M. Dehydrogenative coupling of alcohols to esters on a silica polyamine composite by immobilized PNN and PONOP pincer complexes of ruthenium. *J. Org. Chem.* **2017**, *845*, 213-228.

(40) Tran, B. L.; Johnson, S. I.; Brooks, K. P.; Autrey, S. T. Ethanol as a Liquid Organic Hydrogen Carrier for Seasonal Microgrid Application: Catalysis, Theory, and Engineering Feasibility. *ACS Sustain. Chem. Eng.* **2021**, *9*, 7130-7138.

(41) Shan, J.; Janvelyan, N.; Li, H.; Liu, J.; Egle, T. M.; Ye, J.; Biener, M. M.; Biener, J.; Friend, C. M.; Flytzani-Stephanopoulos, M. Selective non-oxidative dehydrogenation of ethanol to acetaldehyde and hydrogen on highly dilute NiCu alloys. *Appl. Catal. B: Environ.* **2017**, *205*, 541-550.

(42) Lu, Z.; Gao, D.; Yin, H.; Wang, A.; Liu, S. Methanol dehydrogenation to methyl formate catalyzed by SiO_2-, hydroxyapatite-, and MgO-supported copper catalysts and reaction kinetics. *J. Ind. Eng. Chem.* **2015**, *31*, 301-308.

(43) Huang, X.; Cant, N. W.; Wainwright, M. S.; Ma, L. The dehydrogenation of methanol to methyl formate. *Che. Eng. Process.: Process Intensif.* **2005**, *44*, 393-402.

(44) Ilyas, M.; Ikramullah. Dehydrogenation of cyclohexanol to cyclohexanone catalysed by Y_2O_3/ZrO_2: activation energy. *Catal. Commun.* **2004**, *5*, 1-4.

(45) Liu, C.; Li, T.; Dai, X.; Zhao, J.; He, D.; Li, G.; Wang, B.; Cui, X. Catalytic Activity Enhancement on Alcohol Dehydrogenation via Directing Reaction Pathways from Single- to Double-Atom Catalysis. *J. Am. Chem. Soc.* **2022**, *144*, 4913-4924.

(46) Nielsen, M. Catalyst Kinetics and Stability in Homogeneous Alcohol Acceptorless Dehydrogenation. In *Advanced Chemical Kinetics*, **2018**, 129 pages.

(47) Alberico, E.; Lennox, A. J.; Vogt, L. K.; Jiao, H.; Baumann, W.; Drexler, H. J.; Nielsen, M.; Spannenberg, A.; Checinski, M. P.; Junge, H.; et al. Unravelling the Mechanism of Basic Aqueous Methanol Dehydrogenation Catalyzed by Ru-PNP Pincer Complexes. *J. Am. Chem. Soc.* **2016**, *138*, 14890-14904.

(48) Hakim Siddiki, S. M. A.; Toyao, T.; Shimizu, K.-i. Acceptorless dehydrogenative coupling reactions with alcohols over heterogeneous catalysts. *Green Chem.* **2018**, *20*, 2933-2952.

(49) Popov, D. A.; Luna, J. M.; Orchanian, N. M.; Haiges, R.; Downes, C. A.; Marinescu, S. C. A 2,2′-bipyridine-containing covalent organic framework bearing rhenium(i) tricarbonyl moieties for CO_2 reduction. *Dalton Trans.* **2018**, *47*, 17450-17460.

(50) Zhang, S.; Fan, Q.; Xia, R.; Meyer, T. J. CO_2 Reduction: From Homogeneous to Heterogeneous Electrocatalysis. *Acc. Chem. Res.* **2020**, *53*, 255-264.

(51) Huang, Y.; He, H.; Liu, J.; Thummel, R. P.; Tong, L. Electrocatalytic CO_2 Reduction by Molecular Ruthenium Complexes with Polypyridyl Ligands. *Chem. Asian J.* **2022**, *17*, e202200217.

(52) Xia, Q.; Jin, X.; Zhang, G.; Liu, M.; Wang, J.; Li, Y.; Fang, T.; Ding, J.; Zhang, D.; Meng, K.; et al. Catalytic Deoxygenation of Xylitol to Renewable Chemicals: Advances on Catalyst Design and Mechanistic Studies. *Chem. Rec.* **2021**, *21*, 133-148.

(53) Aroua, M. K.; Cognet, P. Editorial: From Glycerol to Value-Added Products. *Front. Chem.* **2020**, *8*, 1-2.

TOC Figure

Heterogenization of Homogeneous Ruthenium(II) Catalysts for Carbon-Neutral Dehydrogenation of Polyalcohols

Ashley N. Hellman, Michael E. Foster, Chaochao Dun, Joseph E. Reynolds III, Christine J. Yu, Andrew D. Trinh, Mohana Shivanna, Ji Yang, Yi Chen, Ji Su, Jeffrey J. Urban, Mark D. Allendorf,* and Vitalie Stavila*

* mdallen@sandia.gov ; vnstavi@sandia.gov